Indian Journal of Chemical Technology
Vol. 31, July 2024, pp. 581-592
DOI: 10.56042/ijct.v31i4. 5707

Improving bubble column modelling by using hybrid multiphase simulation with refined mesh and reformed sparger

Ashish Gaurav* & Prakash Chandra

Department of Mechanical Engineering, National Institute of Technology Patna, Bihar - 800005, India

*E-mail: ashishgauraviith@gmail.com (AG), prakash@nitp.ac.in (PC)

Received 21 September 2023; accepted 2 April 2024

Gas-liquid contactors like bubble columns are crucial in chemical industries, yet conventional meshing methods often overlook local fluctuations, hampering accurate simulation of viscosity's damping effect on bubble behaviour. This leads to reduced gas hold-up and constrained mass transfer rates. To address these issues, a novel Computational Fluid Dynamics approach named Hybrid Multi-Phase Modelling with a Refined Mesh and Reformed Sparger is proposed. This method integrates a Refined Exterior Prismatic Hexahedral Core Mesh, combining unstructured hexahedral and prism meshes to accurately model fluid flow and bubble interactions. Global adaptive mesh refinement enhances simulation accuracy by refining mesh interfaces based on local error estimation. Additionally, a Pento-Centric Conical Orifice Sparger is introduced to produce smaller continuous bubbles and uniformly distribute them, increasing gas holdup and reducing turbulence. Finally, a Hybrid Volume of Flow with Discrete Element Method (VOF-DEM) is employed to address complex geometries, distinguishing phase interfaces with VOF and considering viscosity effects with DEM. Comparative analysis with existing techniques reveals significant improvements: skewness reduced to 0.07, orthogonal velocity increased to 0.98, and liquid velocity reached 0.25 m/s. Overall, this approach enhances gas-liquid contactor simulations, offering improved accuracy and performance in predicting bubble behaviour and mass transfer rates.

Keywords: Bubble column, Bubble Distributor, Gas hold up, Mass transfer rate, Refined mesh, Viscosity

Introduction

Bubbles and cavities are widely utilized in various fields such as ocean and mechanical engineering, biology, chemistry, and military applications. Extensive research since Lord Rayleigh's pioneering work has elucidated the complex dynamics of bubbles generated by diverse sources like cavitation, underwater explosions, and flows. Understanding bubble behaviour and gas-liquid interactions is crucial for optimizing processes and equipment performance[1-3]. Bubble columns (BC) find wide industrial use due to advantages like improved temperature control, low pressure drop, and high heat transfer rates. They offer increased interfacial area, low cost, and ease of operation. However, scaling up requires understanding hydrodynamic and heat transport characteristics, influenced by operating conditions and column design. Gas flow governs BC hydrodynamics, with gas holdup being a critical parameter[4-7]. Gas-liquid characteristics, flow velocity, bubble size, and distributor design significantly influence bubble column flow structure. Gas holdup, a key metric for hydrodynamic properties, correlates strongly with bubble size and gas velocity. Hydrodynamic factors like gas distributor type, column dimensions, and liquid properties further affect these parameters. Despite their simplicity, bubble columns exhibit complex hydrodynamics due to micro- and mesoscale phenomena like bubble deformation and interactions. Successful modelling relies on selecting appropriate empirical models that capture mass, momentum, and turbulence transfer accurately. Industrial system modelling faces challenges due to diverse liquid phases containing substances like fermentation media or solid particles[8-11]. Computational Fluid Dynamics (CFD) simulation is effective for predicting gas-liquid flow in bubble column reactors, yet challenges persist, especially at higher gas velocities and holdup. Sensitivity to sub-models like lift and drag forces, turbulence models, and grid resolution complicates accurate simulation. Describing interphase momentum transfer, particularly lift forces, remains difficult due to complex bubble behaviour. While some studies address lift force modelling, determining the lift coefficient remains challenging. Despite its importance, lift force is often overlooked in CFD simulations. Grid resolution impacts solution convergence and accuracy in solving

computational models' partial differential equations. Maintaining mesh quality is crucial for solution accuracy and convergence[12-15]. Despite advancements in bubble dynamics studies, further challenges persist in refining simulations to align closely with experimental results, crucial for understanding bubble behaviour across diverse applications.

Abdulrahman *et al*.[16] utilized CFD to estimate overall gas holdup in a helium-water bubble column, revealing that increasing superficial gas velocity enhances gas holdup, while increasing static liquid height reduces it. Validation against experimental data demonstrated the applicability of the CFD simulations, although some underestimation occurred due to turbulent flow eddies. Tao *et al*.[17] conducted experiments to distinguish between large and small bubbles and developed a CFD-PBM coupling model to study gas holdup in gas-liquid two-phase flow. They found that increasing surface gas velocity led to rapid increases in gas holdup for both bubble sizes. However, meshing intricacies influenced simulation results and computational time. Guan *et al*.[18] introduced a drag model for effective drag coefficient prediction based on the Dual-Bubble-Size model, showing improved accuracy in gas holdup prediction. However, lack of experimental validation for liquid velocity measurement limited model assessment. Mosavi *et al*.[19] integrated CFD with an adaptive network-based fuzzy inference system to predict flow characteristics in bubble column structures. While increasing input variables improved prediction accuracy, data limitations constrained the model's performance. Ge *et al*.[20] proposed a CFD-Discrete Element Method model for simulating particle swarm interaction with bubbles, revealing decreasing collision efficiency with increasing solid fractions. However, turbulence induced by higher bubble Reynolds numbers increased collision efficiency for greater solid fractions. Bose *et al*.[21] predicted and optimized bubble column performance for photosynthetic biogas upgrading using response surface methodology, demonstrating adequate prediction within specified parameter ranges. Tian *et al*.[22] introduced a method combining computational fluid dynamics with adaptive neuro-fuzzy inference system to predict fluid conditions, offering efficient data classification but limited by the appropriateness of geometric inputs. Manjrekar *et al*.[23] developed a bubble column model integrating optical probe data with machine learning algorithms for flow regime classification, demonstrating effective prediction capabilities but facing challenges in bubble time distribution calculation. Asil *et al*.[24] investigated the impact of various parameters on gas holdup in bubble columns, revealing effects of superficial gas velocity, solid concentration, and sparger type on gas holdup. However, they noted the limitations of certain correlations in predicting gas holdup accurately. Bae *et al*.[25] studied the impact of distributor shape on bubble properties in pressurized bubble columns, revealing variations in microbubble generation and gas holdup based on distributor geometry. Khodabandeh *et al*.[26] analyzed laminar flow of a water nanofluid in microchannels with complex geometries, showing enhanced heat transfer due to improved mixing. However, the study was limited to laminar flow conditions. Toghraie *et al*.[27] investigated convective heat transport in a water-Al_2O_3 nanofluid through a micro concentric annulus, comparing different models for heat transfer enhancement. However, lack of experimental validation and assumptions in the numerical model limited the study's applicability.

Various approaches have been employed to study heat transfer, gas holdup, and flow characteristics in bubble columns and similar systems, each with its limitations. Thus, there is a demand for a mesh type, sparger, and simulation methods to enhance bubble dynamics in fluid columns and address these challenges. There are few specific points are considered in this paper. To accurately capture the damping effect of fluid’s viscosity, a Refined Exterio Prismatic Hexahedral Core Mesh is introduced which combines unstructured hexahedral and prism meshes to accurately simulate fluid flow and bubble interactions in multi-phase systems. The global adaptive mesh refinement algorithm improves simulation accuracy by refining the interface between two mesh types. To tackle turbulent flow and uneven bubble distribution, the Pento-Centric Conical Orifice Sparger is utilized, which features a Conical-shaped Bubble Distributor for generating smaller continuous bubbles, and the Pento-centric arrangement ensures uniform bubble dispersion, thereby minimizing coalescence and turbulence in the fluid column. To accurately reconstruct interface curvature in complex geometries, the Hybrid VOF-DEM is introduced in CFD. Which utilizes VOF for free surface flow analysis and DEM for bubble tracking and collision resolution thereby effectively distinguishing phase interfaces and capturing diverse bubble shapes with viscosity effects. Overall, by following the above

proposed approach aims to enhance bubble dynamics specification, addressing limitations in multi-phase flow to improve bubble column performance.

Hybrid multi-phase modelling with a refined mesh and reformed sparger

Bubble columns are cylindrical or rectangular tubes or vessels used to create bubbles in liquids and analyze their behaviour. The Multi-Phase flow involving the bubbling of liquid with gases is utilized in many industrial processes, especially in bubble columns for improving heat and mass transfer rates. Therefore, there is a need to numerically analyze the dynamic rising characteristics of multiple bubbles to determine their interactions for improving the performance of practical fluid bubble columns. The prediction of the path and velocity of the bubble and the accuracy of the simulation depends on the quality of the mesh and its type in the existing approach. Hence, a novel Computational Fluid Dynamics Approach is introduced namely Hybrid Multi-Phase Modelling with a Refined Mesh and Reformed Sparger to improve the performance of bubble columns and the accuracy of numerical simulations. In the existing approaches structured and unstructured mesh types involved a lack of continuity between the cells and could not capture the local variations which cannot model the dampening effect of fluid's viscosity on the shape and trajectory of the rising bubbles accurately. A new Refined Exterio Prismatic Hexahedral Core Mesh is made up of a Hybrid unstructured hexahedral mesh and a Prism mesh, and it is utilized to simulate fluid flow and bubble interactions in a multi-phase flow.The core part of the fluid column is provided using Unstructured Hexahedral Mesh, which contains high-density cells that provide superior neighbour-cell interaction and thus local variation with all flow properties is effectively treated. The fluid region along the column's wall is given with an Unstructured Prism Mesh type, in which the elements are finely orientated along the fluid column's wall, effectively specifying the velocity gradient and no-slip condition at the wall-fluid interface. To refine the region of the interface between these two mesh types, the Global adaptive mesh refinement algorithm is used, which uses the error estimation strategy to determine the point in the modeling domain where the local error is greatest and then uses this error estimation to generate an entirely new mesh without changing the type of mesh. The interfacial area between gas and liquid determines the shape of the bubble, which is mostly impacted by the type of gas distributor (Sparger). Because of the coalescence and break-up of bubbles in the column, the conventional sparger design provides a very turbulent flow regime and intermittent bubble distribution. As a result, a Pento-Centric Conical Orifice Sparger is introduced, which employs a Conical-shaped Bubble Distributor with a very small orifice diameter (0.5 mm) to create smaller-sized continuous bubbles, hence enhancing gas hold-up. Conical orifices are fitted on the five corners and around the center of a hexagon to give a uniform distribution of bubbles across the bubble distributer surface in a Pento-Centric Arrangement. Furthermore, the existing approaches could not reconstruct the curvature of the interface in complex geometries (Liquid-Bubble interface) since most models (Eulerian models) employ an interpenetrating continuum approach and these approaches require the bubble sizes to be given. In the CFD (Computational Fluid Dynamics), a Hybrid Multiphase Modelling named Hybrid VOF-DEM is introduced in which the VOF (Volume of Flow) approach is used for separated and free surface flow analysis in which the phase interface is solved by the continuity equation as a function of the volume fraction and thus the bubble-fluid characteristics are effectively distinguishable in the multi-phase flow. The DEM (Discrete Element Method) is integrated with the VOF technique in this approach, which considers the influence of viscosity on the bubble liquid interface by using buoyancy and drag forces on each bubble. It also continually follows the bubbles within the bubble column throughout time to solve the trajectories of individual bubbles and their collisions.

Fig. 1 depicts the overall flow diagram of multi-phase modeling with a refined mesh and reformed sparger, in that the bubble column is created, and the sparger is used to produce the bubbles. For the creation of continuous bubbles that are smaller in size, a sparger is used. It consists of a conical bubble distributor with an extremely small orifice diameter of roughly 0.5 mm. To create an even dispersion of bubbles across the bubble distributer area, conical orifices are fitted on the five corners and around the center of a hexagon in pento-centric arrangements. By introducing a Refined Exterio Prismatic Hexahedral Core Mesh where a wide range of fluid flow and particle (Bubbles) interactions occur, the fluid's viscosity on the ascending bubbles in the bubble column is well established. High-density cells in the

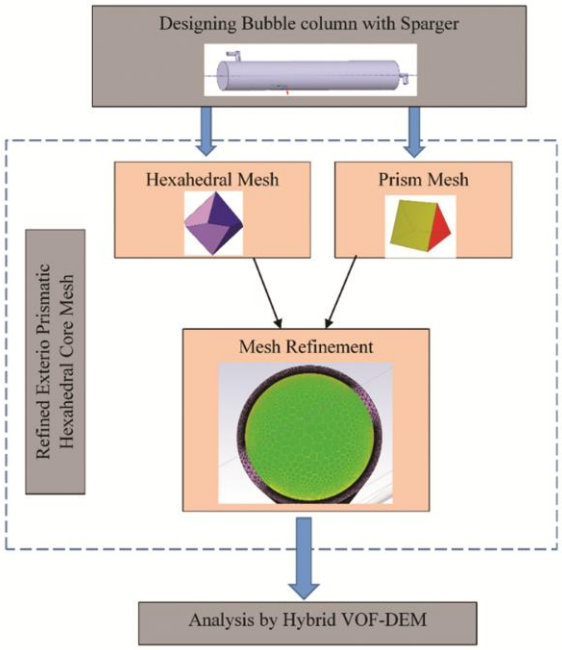

Fig. 1 — Overall flow diagram of Multi-Phase Modeling with a Refined Mesh and Reformed Sparger

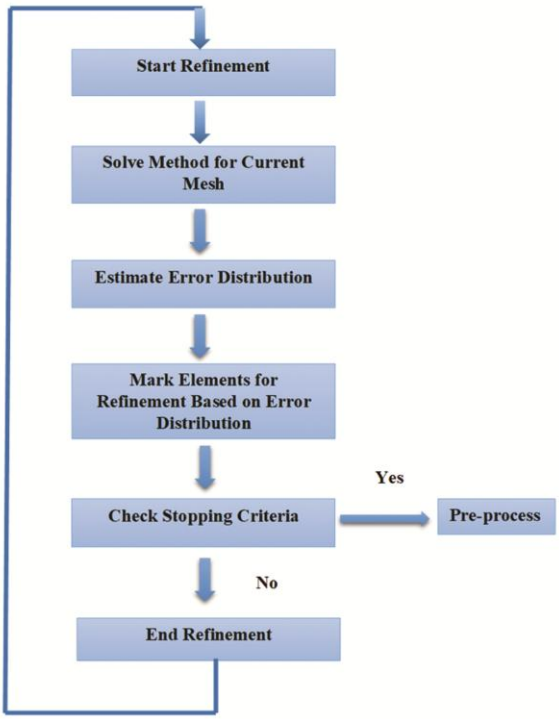

Fig. 2 — Flowchart of mesh refinement process of adaptive mesh algorithm

hexahedral mesh enable improved neighbour-cell interaction and, consequently, local variation. Then, Prism mesh is used to precisely align the elements along the fluid column's wall. To refine the region of the interface of these two mesh types the Global adaptive mesh refinement algorithm is utilized. The curvature of the interface in complex geometrics is reconstructed using the Hybrid VOF-DEM approach which involves different sizes of bubbles with varying shapes and the effect of viscosity on the bubble liquid interface.

The characteristics of multiple bubbles and their interaction are studied in various viscous fluids such as water, olive oil, and honey with a temperature of 25℃ with this novel meshing and hybrid modeling approach and the simulation performance is improved by this novel approach.

Prismatic Hexahedral Core Mesh

In a hybrid mesh composed of both hexahedral and prismatic components, neighbor connection and local variation are critical for accurately simulating flow processes in complex geometries with boundary layer resolution. When modeling flow processes in intricate geometries with boundary layer resolution, hybrid meshes made of both hexahedral and prismatic parts are essential. By using hexahedral components in the bulk flow domain and prismatic elements in the boundary layer region, this method enables more effective and precise simulations. The Prismatic Hexahedral Core mesh generation method recognizes and labels each face of the prismatic and hexahedral elements. A prismatic element has three faces (top, bottom, and lateral) whereas a 3D hexahedral element has six faces (top, bottom, front, back, left, and right). Based on shared faces, the link between hexahedral and prismatic elements is constructed. Each face of a hexahedral element is examined to see if any nearby prismatic elements share a face with it, and vice versa. A connection link between two prismatic elements is established when the face of a hexahedron and a prismatic element share a face. Data structures or arrays are used to hold connectivity-related information. Particularly in regions with large changes in flow parameters, accurate neighbor connectivity is required for the correct computation of fluxes, gradients, and other interactions between hexahedral and prismatic elements, which is essential for accurately capturing flow physics.

During the coupling of various mesh types, the interface between two different mesh types needs to be refined. At an interface where hexahedral mesh and prism mesh cross, it is crucial to provide correct and seamless communication.An adaptive mesh refinement method generally follows the well-established iterative refinement loop based on Fig. 2.

Fig. 2 shows the flowchart of the adaptive mesh algorithm's mesh refinement process. At the beginning of each iteration of refinement, a discrete operation is performed to produce a conforming locally refined mesh, such as the prismatic and hexahedral. The error estimator then calculates the error of the mesh refinement procedure. Thus, based on the variation between a reconstructed smoothed gradient, the element-wise error distribution is evaluated. The marking strategy uses an element-wise error field, while global adaptive mesh refinement uses parametric detection for hexahedral and prism mesh refinement. This procedure entails defining a maximum permissible elementary error based on various distributional considerations.The predicted error is weighted about the total energy of the strain that results from adding the elementary contribution. The process of refining continues until the finishing of the interface between the two meshes, at which STOP indicates whether halting criteria have been met or not. If it meets the halting criteria then it moves on to the process of computing the numerical simulation.

Algorithm 1: Adaptive mesh refinement algorithm

Adaptive mesh refinement (AMR) is a technique used for adjusting the precision of a solution inside particular delicate or turbulent regions on simulation. When solutions are calculated numerically, they are frequently constrained to quantized grids that have been predetermined, such as the Cartesian plane, which makes up the computing grid, or "mesh."

Input: user-defined local error tolerance ϵΩ, user-defined local volume control parameter δ, initial mesh M_0

Output: Converged numerical solution

Set $i = 0$

$\widehat{M_0} \leftarrow M_0$

boolean**stop**:= false

while not stop do

• U_i := **SOLVE METHOD**M_i $or\{\widehat{M_g}\}_{g=0}^{i}$

•$\{\in T_i\}_{T^i \in M^i}$:= **ESTIMATE($U_i, M_i$)**

•X_i^0:= **MARK**(U_i , $\{\in T_i\}_{T^i \in M^i}$, M_i)

• **stop** := **STOP**($\{\in T_i\}_{T^i \in M^i}$,$X_i^0$, ϵΩ, δ)

if stop = true then exit end if

•$M_{i+1}, \widehat{M}_{I+1}$:= **REFINEMETHOD**($M_i$,$\{\beta_{T^i}\}_{Ti \in Mi}$, $M_i, \widehat{M_i}$)

• i ← i + 1

end while

This algorithm consists of generating a sequence of approximate solutions $\{u_i\}_{i=0}^{k}$which aims to converge toward an acceptable (up to the desired accuracy) solution. Thus, starting from an initial discretization M_0 of a domain $\Omega \subset R^D$, with D being the dimension of the problem, a series of global meshes with more and more locally refined elements $\{M_i\}_{i=1}^{k}$ is produced. The sub-meshes $\widehat{M_i}$, $1 \le i \le k$, gather the refined elements of refinement step i ($\widehat{M_i} \subset M_i$). The solution U_k approximated on the last mesh M_k aims to satisfy the prescribed accuracy requirements. Let T_i be an element of the mesh M_i, $0 \le i \le k$. Relying on common steps included within the refinement procedure depicted in Fig. 2, we propose a generic fully automatic refinement algorithm applicable to the considered AMR methods. The refinement process aims to satisfy a user-defined accuracy by verifying (at each refinement iteration) the achieved local error tolerances.

Pento-centric conical orifice sparger

The interfacial area between gas and liquid, which is primarily influenced by the type of gas distributor (Sparger), is a key determinant of the gas hold-up, which determines the shape of the bubble. The Pento-centric conical orifice sparger outlet was considered as the air entry to the column and its size was used to compute the velocity of the air flow. To distribute bubbles evenly across the bubble distributer area, avoid bubble coalescence and breakup, and minimize turbulent flow patterns inside the fluid column, these conical bubble distributors are designed in a Pento-Centric Arrangement, in which the Conical orifices are provided on the five corners, and around the center of a hexagon. The computational domain included tailings pipe and pulp zone disregarding the froth zone. Through studies, the valve of the feed inlet pipe was assumed to be closed and only air was directed to the column filled with pulp. A specific type of gas dispersion device used in industrial processes like chemical reactions, wastewater treatment, and fermentation is called a conical orifice sparger with a penta-centric layout. The use of a conical-shaped bubble distributor with an orifice diameter allows the generation of continuous bubbles that are smaller in size, which boosts the gas hold-up. Fig. 3 provides the design of the sparger which is used to inject gas into a liquid medium to produce bubbles that improve mixing and mass transfer between the

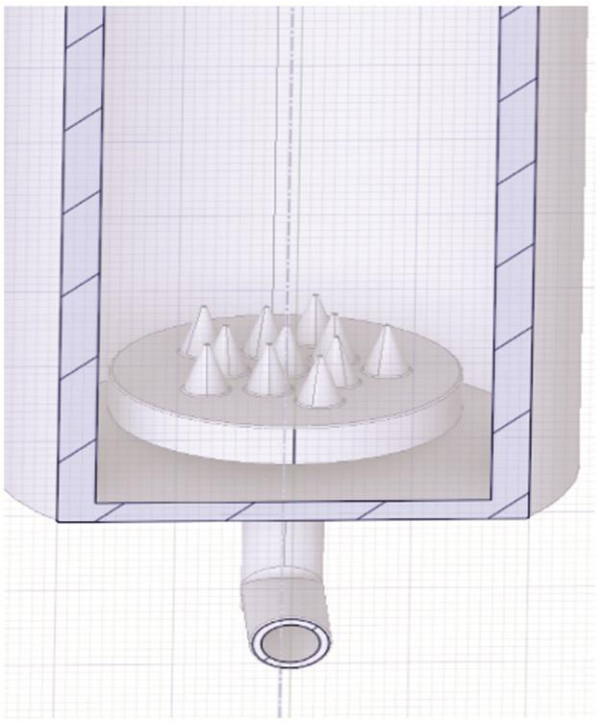

Fig. 3 — Design of Pento-centric conical orifice sparger

gas and the liquid. Air is used as the gas in this apparatus.

The major part of the apparatus is the conical orifice sparger. Typically, it consists of a plate or nozzle with a conical shape and tiny orifices (holes) through which the gas is injected into the liquid. The conical shape aids in concentrating the gas flow, which improves bubble distribution and production in the liquid media. The process-specific requirements, gas flow rates, and desired bubble size distribution all affect the specific configuration that is used. The orifices are arranged in a five-point layout, which is referred to as a "penta-centric" arrangement. The conical orifice sparger has five orifices in this design, which are symmetrically spaced around its axis. By ensuring consistent gas distribution and bubble production inside the liquid, this design enhances mixing and mass transfer efficiency.

Hybrid VOF-DEM (Volume of Flow with Discrete Element)

To approximate the transient air–water interface, while tracking it on the Prismatic Hexahedral Core mesh, the classical VOF-DEM method is utilized. This technique was demonstrated to be very efficient when dealing with the complex interface between multi-phase flow fluids and has been widely used to investigate droplets.

Volume configuration of each phase in a computational cell

In a computational cell (V_{cell}), the volumes of gas (V_g) and liquid phases (V_l) meet the following relationship,

$$V_{cell} = V_g + V_l \quad \text{... (1)}$$

The void fraction (ε) and the colour function (α) are introduced to represent the volume fraction of fluid in the cell and the volume ratio of the liquid phase in the fluid, separately[28]. The volume of cells in each phase is expressed as shown in Eq. (2),

$V_g + V_l = \varepsilon V_{cell}$ (2)

Where, $V_g = (1-\alpha)\,\varepsilon V_{cell}$ and $V_l = \alpha\varepsilon V_{cell}$

Governing equations of fluid phase

Due to lower gas and liquid velocities, the multi-phase flow is dominant in the gas-liquid fluidized bed which is described using the volume-average NavierStokes [28] equations given in Eqs (3) and (4),

$$\frac{\partial(\varepsilon)}{\partial t} + \nabla \cdot (\varepsilon U) = 0 \quad \text{... (3)}$$

$$\frac{\partial(\varepsilon\rho_f U)}{\partial t} + \nabla \cdot \left(\varepsilon\rho_f UU\right)) - \nabla \cdot (\varepsilon\tau) = \varepsilon\,(-\nabla p + \rho_f g + F_\sigma\,) + F_{fp} \quad \text{... (4)}$$

By introducing ε both in the continuity and momentum equations, the conservations of mass and momentum are established based on the volume of fluid in the grid. τ is the stress tensor of fluid, and in the case of viscous multi-phase flow which is given in Eq. (5),

$$\tau = \mu_f(\nabla U + \nabla U^T) \quad \text{... (5)}$$

U, ρ_f, and μ_f are the velocity, density, and viscosity of the fluid in a computational cell, respectively. ρf and μf are the linear interpolations of the physical properties of liquid and gas phases mentioned in Eqs (6) and (7).

$$\rho_f = \alpha\rho_l + (1-\alpha)\rho_g \quad \text{… (6)}$$

$$\mu_f = \alpha\mu_l + (1-\alpha)\,\mu_g \quad \text{… (7)}$$

F_{fp} is the reaction force on the fluid derived from the momentum exchange with the bubble. F is the volumetric force generated by the additional pressure gradient due to the surface tension at the gas–liquid interface in the corresponding region. Its value is quantified by the CSF (continuum surface force) model in Eq. (8).

$$F_\sigma = \sigma k \nabla\alpha \quad \text{… (8)}$$

where σ and k are the surface tension of the liquid phase and the curvature of the gas-liquid interface in a computational cell, respectively. The curvature of the phase interface in a computational cell is given by Eq. (9).

$$k = \nabla \cdot n \quad \ldots (9)$$

n is the normal vector computed from the gradient of the smoothed colour function ($\nabla\alpha$) which is given in Eq. (10),

$$n = -\nabla\alpha/|\nabla\alpha| \quad \ldots (10)$$

Transport equation for interface

In the VOF method, the movement of the gas-liquid interface is governed by the transport[28] equation given in Eq. (11).

$$\frac{\partial(\alpha)}{\partial t} + \nabla \cdot (\alpha U) = 0 \quad \ldots (11)$$

The fluid in the cell with α = 1 is the liquid phase, and it is the gas phase in the case of α= 0. The gas-liquid interface is located at the cells where 0 <α< 1.

Governing equations of Bubble motion

The motions of particles including translation and rotation, as well as the inter-particle and particle-wall collisions, are described by the DEM equations[28] given in Eqs (12) and (13).

$$mp\ \frac{dv_i}{dt} = \sum_j F(c,ij) + m_p g + F_{pf} \quad \ldots (12)$$

$$I_p \frac{d}{dt} = \sum_j T(c,ij) \quad \ldots (13)$$

where m_p, g and I_p are the mass, gravitational acceleration, and rotational inertia of the particle, separately. v_i and w_i denote the translational and angular velocities of the i^{th} particle, separately. $F(c,ij)$ and $T(c,ij)$ is the contact force and torque acting on the i^{th} particle by the j^{th} particle or wall. F_{pf} is the interaction force of particles with fluid, which will be explained in the following section. Furthermore, all particles are traced by their trajectories obtained from the numerical integration of DEM equations.

Calculation of void fraction

In the combination of VOF and DEM, to accurately delineate the gas-liquid interface, the grid size must be very small. Hence, in this study, the grid size has to be reduced to small enough which results in a low average grid-to-particle size ratio of 1:11. In this case, the grid size is close to the particle diameter, while individual particles are typically accommodated by multiple grids. Therefore, a particle dividing model was used for computing the void fraction[28], i.e., the particle was divided by the mesh surface and only the portion of the particle contained in the grid was used to calculate the void fraction of that grid. In addition, a porous particle model was adopted to further improve the local continuity of the void fraction field. Details about this model can be found in the Supplementary Information.

$$\varepsilon = 1 - \frac{V_s}{V_{cell}} 0 \quad \ldots (14)$$

Fluid-Bubble interaction

The fluid in a grid interacts with the particles present in that grid and is responsible for the reaction force of the particles on the fluid (F_{fp}) andthe body force from the fluid acting on each particle(F_{pf}) whose centroid is located in that grid and it is assumed to be exerted on the centroid of the particle, thus there is no torque generated from it on the particle surface. F_{pf} is the sum of various forces from the action of fluid onto particles, and in this paper, it involves the pressure gradient force ($F\nabla p$), virtual mass force (Fv), and drag force (F_d). Furthermore, in the case of the mini-fluidized bed with a single bubble, the particles cannot penetrate the gas–liquid interface into the small bubble due to the strong surface tension of the mini-bubble. To conform to the real situation, it is considered that the interaction between the fluid and the particles is dominated by the direct effect of the liquid phase, while the interaction of the bubble (gas phase) and particles is indirectly reflected by the momentum exchange of the bubble with surrounding liquid phase[28]. Therefore, the following three forces are calculated based on the role of the liquid phase. $F\nabla p$ contains the buoyancy force generated from the hydrostatic pressure difference on the particles, and it is given in equation (15).

$$F\nabla p = -V_p \nabla P \quad \ldots (15)$$

V_p is the particle volumeandF_v is the reaction force of the liquid acting on the particles when the motion of the bubble accelerates the liquid phase which can be calculated from Eq. (16).

$$F_v = k_v V_p \rho_l \frac{d\,(u - v)}{dt} \quad \ldots (16)$$

k_v is a coefficient determined from an empirical correlation, ρ_l is the density of the liquid and u is the linear interpolation of the fluid velocity (U) at the

centroid of the bubble. As for F_d, the equation is given by,

$$F_d = \frac{\beta V_p}{1-\epsilon}(u - v) \quad \ldots (17)$$

Where β is the particle shape factor. Thus, the equations for F_{fp} and F_{pf} are given in Eqs (18) and (19), respectively,

$$F_{pf} = F_{\nabla p} + F_v + F_d \quad \ldots (18)$$

and,

$$F_{fp} = \frac{\sum \gamma_i F_{pf,i}}{V_{cell}} \quad \ldots (19)$$

$F_{pf,i}$ is the force exerted on the i^{th} particle in the grid by the fluid. F_{pf} is the reaction force on the fluid according to the volume fraction of the particles in the grid γ.

Overall, the hybrid unstructured hexahedral and prism mesh improves the mesh technique. In the area of the interface, these meshes are refined using the global adaptive mesh refinement process. By creating a conical-shaped bubble distributor with a pento-centric arrangement that prevents the interruption of bubble distribution, the gas hold-up is improved. Then, by applying Hybrid VOF-DEM, this work efficiently acquires both the phase interface and the variety of bubble forms that are related to viscosity.

Results and Discussion

The results obtained from the proposed model have been provided in this section. The results showed that the proposed model selects the Hybrid mesh type with the optimized thickness will withstand the factors reducing the absorption of light energy and the increase in efficiency of the proposed approach is also proved by comparing it with other existing approaches.

System Requirements

OS	: Windows 10 Pro
Processor	: Intel(R) Core(TM) i3-4130 CPU
RAM	: 8GB
Tool	: Ansys CFD 2021 R2

Simulation results

In this proposed method unstructured hexahedral and prism mesh are utilized to capture the local variations and maintain the continuity between the cells. Conical bubble distributors are designed in a Pento-Centric Arrangement to improve the gas hold up which is responsible for the bubble shape.

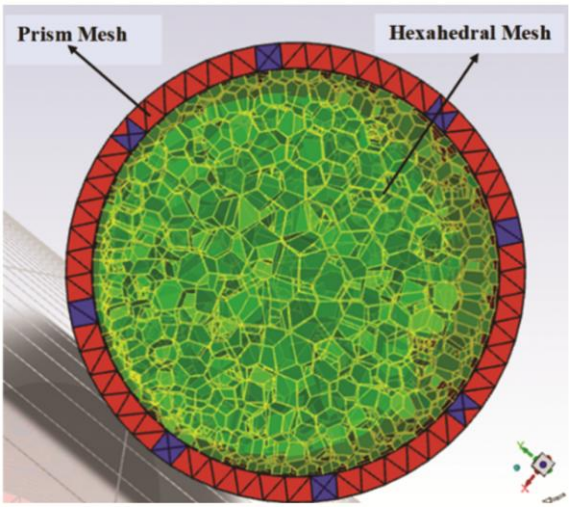

Fig. 4 — Refined Exterio Prismatic Hexahedral Core Mesh

Fig. 4 shows the novel Refined Exterio Prismatic Hexahedral Core Mesh. The numerical simulations were carried out on a 3D unstructured hexahedral mesh and a prismatic mesh. To determine whether the findings were dependent on the cell size, a mesh independence analysis was carried out. It was shown that a small amount of computational cost may be saved. Due to the adoption of three prism layers and the existence of minor geometrical details and a complicated flow field near the wall (where boundary layer gradients were captured), and near the sparger (where boundary layer gradients were also captured), the was refined in these areas. It was also made sure that the grid quality was good during the mesh generation process because discretization of bad quality might lead to both convergence issues and erroneous physics descriptions. The quality parameter values are within a desirable range. Most cells have very high orthogonal quality values, and only a small number of cells have lower quality.

Fig. 5 displays the profiles of the turbulent kinetic energy of the three fluids. The simulated values of the three fluids are compared with each other in the bubble column. The deviation of the simulated results of the Honey is the largest with the instantaneous contour of turbulent kinetic energy with 9.994×10^{-1} m^2s^2, Olive oil is less than the Honey but greater than the Water with 9.984×10^{-1} m^2 $s^{-2}$and water is with less turbulent kinetic energy of about 9.898×10^{-1} m^2 s^{-2}. When there is less plume in the bubble column, there is less turbulence. The kinetic energy of the water in a turbulent state rapidly decreases with height. The axial liquid velocity decreases as a result of an

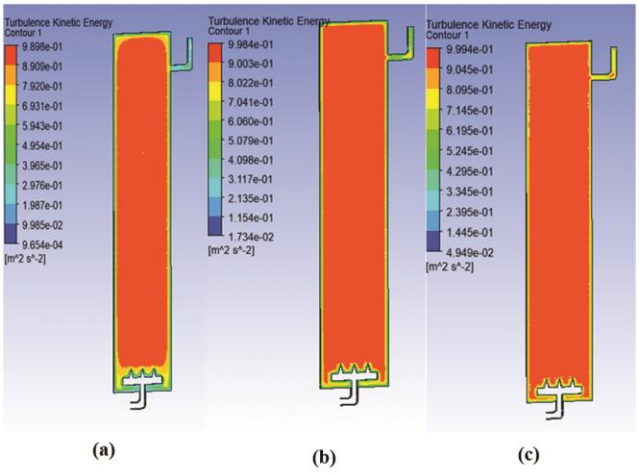

Fig. 5 — Snapshots of turbulent kinetic energy of (a) water, (b) olive oil and (c) honey

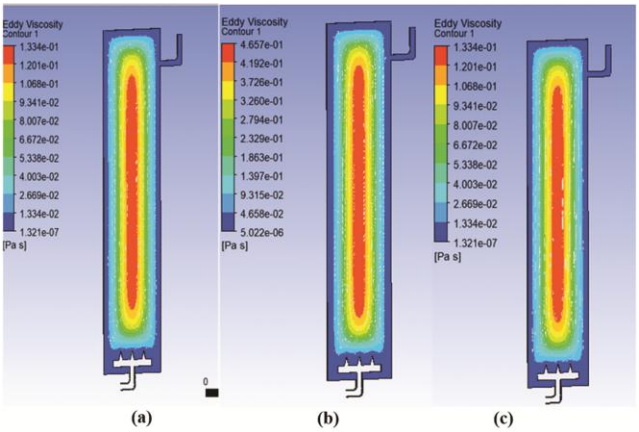

Fig. 6 — Snapshots of Eddy viscosity of (a) water, (b) olive oil and (c) honey

increase in the bubble plume oscillations and honey's liquid phase velocity disturbances.

The results of three distinct fluids' simulations of turbulent viscosity in turbulence models are shown in Figure 6. According to Fig. 6, the basic patterns of turbulent viscosity distribution at various bubble column heights are similar, being generally flat in the center and rapidly decreasing along the wall. This pattern is increasingly obvious as the height rises. Additionally, it can be noted that at various heights, the turbulent viscosity of honey is 2 times greater than that of olive oil and 3 times greater than that of honey. Water's turbulent or eddy viscosity is 1. 334 x 10^{-1} Pa S, olive oil's eddy viscosity is 4. 657 x 10^{-1} Pa S, and the eddy viscosity of Honey is 6.67 x 10^{-1} Pa S.

Fig. 7 shows the results of density simulated by three different fluids in the turbulence models. From Fig. 7, it can be seen that the buoyancy force exerted

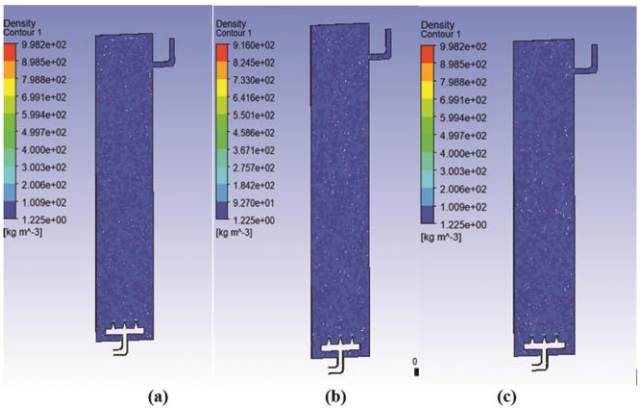

Fig. 7 — Snapshots of density of (a) water, (b) olive oil, and (c) honey

on the gas bubbles is influenced by the fluid's density. Slower bubble rise velocities occur from a decrease in buoyancy force as the liquid phase's density rises. The gas holdup is influenced by the fluid's density because higher-density liquids tend to retain bubbles more effectively. Here, the density of the water is 1.009 x 10^{2} Kg m^{-3}, the density of the olive oil is 9.270 x 10^{2} Kg m^{-3} and the density of the honey is 9.892 x 10^{2} Kg m^{-3} where the gas hold-up is more effective in water. Gas holdup must be properly controlled to maximize reactor performance and gas-liquid mass transfer. Olive oil has a higher viscosity and surface tension compared to water, which may hinder bubble formation and stability. Similarly, honey has much higher viscosity and surface tension than water, making it less favourable for bubble formation and gas holdup.

Overall, the simulation's results show how different factors affect the bubble column's performance and mass transfer rate. Poor performance results from a poorly designed mesh and consideration for the refinement process. The axial liquid viscosity is influenced by factors such as turbulent kinetic energy, eddy viscosity, and density. These factors also have an impact on the development and stability of bubbles.

Comparative analysis of proposed system

This section highlights the proposed Hybrid Multi-Phase Modelling with a Refined Mesh and Reformed Sparger model performance by comparing it to the outcomes of existing approaches such as Coarse mesh, Medium mesh, Fine mesh[29], Cut cell, Polyhedral, Tetrahedral[30], Standard k-ε, RNG k-ε, Realized k-ε, LES[31] and showing their results based on various metrics.

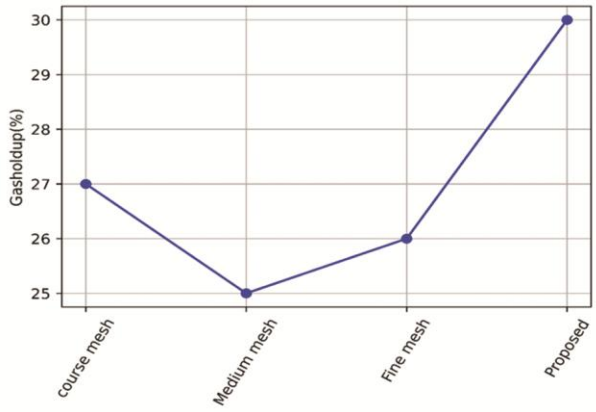

Fig. 8 — Comparative analysis of gas holdup of the proposed model

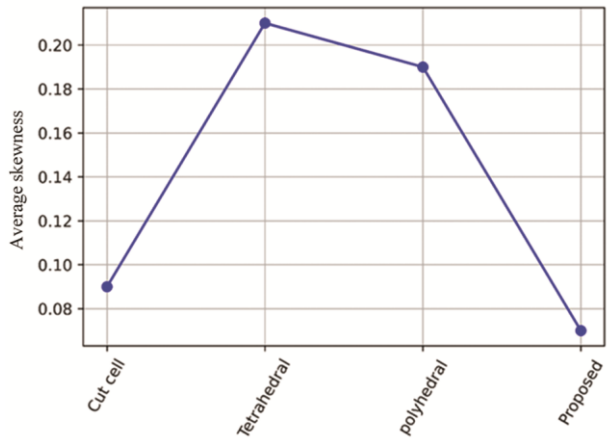

Fig. 9 — Comparative analysis of average skewness of the proposed model

Fig. 8 depicts the comparison of the gas holdup of the proposed approach with existing mesh types[29].The existing mesh types such as Coarse mesh, Medium Mesh, and Fine mesh obtained a Gas hold up of about 27%, 25%,and 26%, and the proposed approach with hybrid hexahedral and prismatic mesh obtained a 30% gas hold up. The gas holdup influences the hydrodynamics of the bubble column, including bubble size distribution and bubble rise velocity. These factors impact column stability, pressure drop, and the possibility of carryover of liquid and gas. This shows hybrid mesh in this proposed approach withstands the factors and the stability of the bubble column is better than the existing approaches.

Fig. 9 depicts the comparison of average skewness of the proposed approach with existing mesh types[30]. The existing mesh types such as Cut cell, tetrahedral, and Polyhedral obtained an Average Skewness of about 0.09, 0.21, 0.19 and hybrid hexahedral and prismatic mesh in this proposed approach obtained

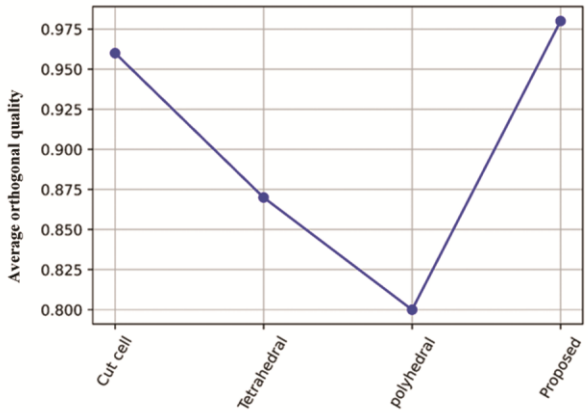

Fig. 10 — Comparative analysis of average orthogonal quality of the proposed model

0.07 which is lower than all other existing methods. Average skewness provides information about the degree of asymmetry in the bubble size distribution. An ideally symmetric bubble size distribution where skewness near zero indicates a relatively uniform distribution of bubble sizes. In this proposed approach skewness is near to zero and the uniform bubble distribution is achieved compared to the existing approaches.

Fig. 10 depicts the comparison of the average orthogonal quality of existing mesh types with the proposed approach. The existing mesh types such as Cut cell, tetrahedral, and Polyhedral obtained an orthogonal quality of about 0.96, 0.87, 0.80 and this hybrid hexahedral and prismatic mesh obtained 0.98 which is higher than all other existing approaches[30]. The magnitude of orthogonal quality influences the rates of bubble coalescence (bubbles merging) and breakup (large bubbles splitting into smaller ones). These processes affect the bubble size distribution and overall bubble population within the column. This shows that the bubble distribution is better with the proposed Pento-centric conical orifice sparger than existing approaches because of higher orthogonal quality.

Fig. 11 depicts the comparison of liquid velocity of the introduced method with existing methods. The existing methods such as Standard k-ε, RNG k-ε, Realized k-ε, *and* LES obtained a liquid velocity of about 0.23 m/s, 0.20m/s, 0.225m/s, 0.21m/s, and the proposed method achieve 0.25 m/s which is better than the other existing approaches[31]. Liquid velocity impacts the rise velocity of gas bubbles. The combined effect of liquid velocity and buoyancy determines how fast bubbles rise through the liquid

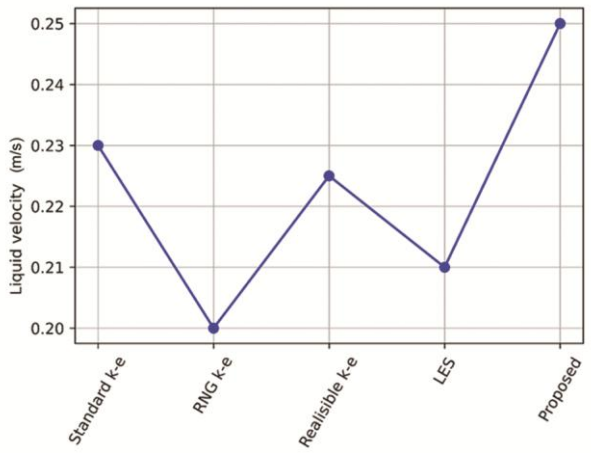

Fig. 11 — Comparative analysis of liquid velocity of the proposed model

phase. This demonstrates that the suggested sparger design provides a better gas bubble rise velocity through the liquid phase which improves the efficiency and performance of this system.

Overall, factors such as the gas hold-up, Skewness, Orthogonal velocity, and liquid velocity in the bubble column show that the gas holdup is improved by distributing smaller bubbles uniformly. Spargers produce smaller bubbles with better stability and with uniform distribution which improves the efficiency and performance of the bubble column.

Conclusion

By examining fluids like water, olive oil, and honey, significant insights into bubble formation and stability are obtained, with viscosity playing a crucial role. Water, characterized by lower viscosity and surface tension compared to olive oil and honey, exhibits superior bubble formation and retention capabilities, owing to its lower density facilitating bubble floatation. The proposed approach achieves about 30% Gas hold up, 0.96 orthogonal velocity, and 0.25 m/s liquid velocity which is higher, and 0.07 skewness which is lower than other approaches and thus improves the efficiency and performance of the bubble column by uniform bubble distribution with the novel sparger design. This research emphasizes optimizing bubble column performance for diverse industrial applications, particularly in chemical, petrochemical, and environmental engineering, to enhance heat and mass transfer rates. Through innovative sparger designs and rigorous assessment of factors influencing gas holdup, orthogonal velocity, and liquid velocity, the proposed approach aims to achieve higher efficiency and performance while ensuring uniform bubble distribution. There is the possibility of experimentation in optimizing sparger designs for bubble columns. Research wanted to look into different sparger geometries, sizes, and configurations to maximize gas holdup while minimizing turbulence, resulting in increased column performance. Future research concentrates on developing even more advanced meshing algorithms for bubble column simulations. This could entail developing new mesh types or improving present ones to better portray the complicated flow dynamics and interactions between bubbles and the surrounding fluid. Future studies investigate into further optimization of hybrid mesh configurations for bubble column simulations. It entails looking into different mesh type combinations, such as using tetrahedral or polyhedral components in addition to hexahedral and prism meshes, to achieve even higher resolution and accuracy in recording flow events.

Supplementary Information

Supplementary information is available on the website http://nopr.niscpr.res.in/handle/123456789.

Reference

1 Laguillaumie L, Rafrafi Y, Moya-Leclair E, Delagnes D, Dubos S, Spérandio M, Paul E & Dumas C, Stability of ex situ biological methanation of H2/CO2 with a mixed microbial culture in a pilot scale bubble column reactor, *Bioresour Technol*, 354 (2022) 127180.

2 Moradi H, Kim D S, Kim S H, Chang Y Y, Yang J K, Choi E H & Kamranifard T, Experimental and numerical study on diazinon removal using plasma bubble column reactor: Modeling, kinetics, mechanisms, and degradation products, *J Environ Chem Eng*, 10 (2022) 108291.

3 Sauerschell S, Bajohr S & Kolb T, Methanation pilot plant with a slurry bubble column reactor: Setup and first experimental results, *Energy Fuels*, 36 (2022) 7166.

4 Sauerhöfer-Rodrigo F, Díaz I, Rodríguez M & Pérez P, Modelling of fixed bed and slurry bubble column reactors for Fischer–Tropsch synthesis, *Rev Chem Eng*, 40 (2024) 151.

5 Noh Y G, Lee Y J, Kim J, Kim Y K, Ha J, Kalanur S S & Seo H, Enhanced efficiency in CO2-free hydrogen production from methane in a molten liquid alloy bubble column reactor with zirconia beads, *Chem Eng J*, 428 (2022) 131095.

6 Li L, Zhao Y, Lian W, Han C, Liu Y, Li P, Zhang Q & Huang W, Insight into the effect of particle density and size on the hydrodynamics of a particular slurry bubble column reactor by CFD-PBM approach, *Powder Technol*, 400 (2022) 117264.

7 Chaturvedi A & Jaiswal R P, Optimization for minimizing the cost of ozonation of highly concentrated textile dyeing wastewater in a bubble column reactor, *Environ Sci Pollut Res*, 29 (2022) 88018.

8 Dong J, Yao J, Tao J, Shi X & Wei F, Degradation of methyl orange by ozone microbubble process with packing in the bubble column reactor, *Environ Technol*, 44 (2023) 2512.

9 Zhang C, Liu Y, Jiao W, Shen H, Yuan X & Jia S, An optimization method for enhancement of gas–liquid mass transfer in a bubble column reactor based on the entropy generation extremum principle, *Chin J Chem Eng*, 53 (2023) 83.

10 Besagni G, Varallo N & Mereu R, Computational fluid dynamics modelling of two-bhase bubble columns: A comprehensive review, *Fluids*, 8 (2023) 91.

11 Lim S H, Kwon H E, Go K S, Pham H H, Nho N S, Kim K H & Kim K D, Estimation of the gas hold up and flow regime of a bubble column reactor for the slurry phase hydrocracking of heavy oil, *Fuel*, 338 (2023) 127190.

12 Kar A & Bahadur V, Analysis of coupled heat & mass transfer during gas hydrate formation in bubble column reactors, *Chem Eng J*, 452 (2023) 139322.

13 Silva A C B, Batista G, Esperança M N, Badino A C & Béttega R, Analysis of the interfacial force effect on simulated oxygen transfer of a bubble column using computational fluid dynamics, *Digit Chem Eng*, 5 (2022) 100061.

14 Nadal-Rey G, McClure D D, Kavanagh J M, Cassells B, Cornelissen S, Fletcher D F & Gernaey K V, Computational fluid dynamics modelling of hydrodynamics, mixing and oxygen transfer in industrial bioreactors with Newtonian broths, *Biochem Eng J*, 177 (2022) 108265.

15 Liu Q, Zhang J, Guan X & Yang N, A new drag model for CFD modeling of bubble columns with surfactant, *Chem Eng J*, 455 (2023) 140682.

16 Abdulrahman M W, CFD simulations of gas holdup in a bubble column at high gas temperature of a helium-water system, *In Proc 7th world Congress on Mech*, *Chem Mater Eng*, *(*2020) 169.

17 Tao F, Ning S, Zhang B, Jin H & He G, Simulation study on gas holdup of large and small bubbles in a high pressure gas–liquid bubble column, *Processes*, 7 (2019) 594.

18 Guan X & Yang N, CFD simulation of bubble column hydrodynamics with a novel drag model based on EMMS approach, *Chem Eng Sci*, 243 (2021) 116758.

19 Mosavi A, Shamshirband S, Salwana E, Chau K W & Tah J H, Prediction of multi-inputs bubble column reactor using a novel hybrid model of computational fluid dynamics and machine learning, *Eng Appl Comput Fluid Mech*, 13 (2019) 482.

20 Ge L, Evans G M & Moreno-Atanasio R, CFD-DEM investigation of the interaction between a particle swarm and a stationary bubble: Particle-bubble collision efficiency, *Powder Technol*, 366 (2020) 641.

21 Bose A, O'Shea R, Lin R & Murphy J D, Optimisation and performance prediction of photosynthetic biogas upgrading using a bubble column, *Chem Eng J*, 437 (2022) 134988.

22 Tian E, Babanezhad M, Rezakazemi M & Shirazian S, Simulation of a bubble-column reactor by three-dimensional CFD: Multidimension-and function-adaptive network-based fuzzy inference system, *Int J Fuzzy Syst*, 22 (2020) 477.

23 Manjrekar O N & Dudukovic M P, Identification of flow regime in a bubble column reactor with a combination of optical probe data and machine learning technique, *Chem Eng Sci*, 2 (2019) 100023.

24 Asil A G, Pour A N & Mirzaei S, Intrinsic hydrodynamic investigation of three-phase bubble column: Comparative experimental study on gas holdup, *Theor Found Chem Eng*, 54 (2020) 331.

25 Bae K, Go G S, Noh N S, Lim Y I, Bae J & Lee D H, Bubble characteristics in pressurized bubble column associated with micro-bubble dispersion, *Chem Eng J*, 386 (2020) 121339.

26 Khodabandeh E, Rozati S A, Joshaghani M, Akbari O A, Akbari S & Toghraie D, Thermal performance improvement in water nanofluid/GNP–SDBS in novel design of double-layer microchannel heat sink with sinusoidal cavities and rectangular ribs, *J Therm Anal Calorim*, 136 (2019) 1333.

27 Toghraie D, Mashayekhi R, Arasteh H, Sheykhi S, Niknejadi M & Chamkha A J, Two-phase investigation of water-Al2O3 nanofluid in a micro concentric annulus under non-uniform heat flux boundary conditions, *Int J Numer Methods Heat Fluid Flow*, 30 (2019) 1795.

28 Li X, Liu M, Dong T, Yao D & Ma Y, VOF-DEM simulation of single bubble behavior in gas–liquid–solid mini-fluidized bed, *Chem Eng Res Des*, 155 (2020) 108.

29 Varallo N, Besagni G & Mereu R, Computational fluid dynamics simulation of the heterogeneous regime in a large-scale bubble column, *Chem Eng Sci*, 280 (2023) 119090.

30 Hussain F, Jaskulski M, Piatkowski M & Tsotsas E, CFD simulation of agglomeration and coalescence in spray dryer, *Chem Eng Sci*, 247 (2022) 117064.

31 Cao Q, Chu D, Zhang J, Bi H, Xuan Y & Li P, Effect of drag laws and turbulence models on CFD modeling of the bubble behavior and fluid flow in RH reactor, *J Miner Metal Mater Soc*, 73 (2021) 2660.